Journal of Renewable Materials

Tech Science Press

DOI: 10.32604/jrm.2023.026397

ARTICLE

Role of Calcination Temperature on Isosorbide Production from Sorbitol Dehydration over the Catalyst Derived from Ce(IV) Sulfate

Medta Boupan[1,2], Kanyapak Prompang[1], Achiraya Chompunuch[1], Piwat Boonma[1], Arthit Neramittagapong[1,2,3,4], Somnuk Theerakulpisut[5] and Sutasinee Neramittagapong[1,2,3,*]

[1]Department of Chemical Engineering, Faculty of Engineering, Khon Kaen University, Khon Kaen, Thailand

[2]Research Center for Environmental and Hazardous Substance Management (EHSM), Khon Kaen University, Khon Kaen, Thailand

[3]Center of Excellence on Hazardous Substance Management (HSM), Pathumwan, Bangkok, Thailand

[4]Center of Excellence on Catalysis and Catalytic Reaction Engineering (CECC) Chemical Engineering, Faculty of Engineering, Chulalongkorn University, Patumwan, Bangkok, Thailand

[5]Energy Management and Conservation Office, Faculty of Engineering, Khon Kaen University, Khon Kaen, Thailand

[*]Corresponding Author: Sutasinee Neramittagapong. Email: sutasineene@kku.ac.th

Received: 20 September 2022 Accepted: 19 October 2022 Published 07 June 2023

ABSTRACT

Isosorbide is a multi-purpose chemical that can be produced from renewable resources. Specifically, it has been investigated as a replacement for toxic bisphenol A (BPA) in the production of polycarbonate (PC). In this study, the synthesis of isosorbide by sorbitol dehydration using a cerium-based catalyst derived from calcined cerium (IV) sulfate (300°C, 400°C, 450°C, 500°C, and 650°C) was investigated. The reaction occurred in a high-pressure reactor containing nitrogen gas. Advanced instrumental techniques were applied to analyze the characteristics of the calcined catalyst. The results showed that the calcined catalysts demonstrated different crystalline structures and sulfate species at different temperatures. However, the acidic properties (strength and amount) of the catalyst did not change with the calcination temperature. The cerium (IV) sulfate calcined at 400°C exhibited the best catalytic performance, achieving the highest isosorbide yield (55.7%) and complete conversion of sorbitol at 180°C, 20 bar of N_2, and 6 h using CeSO-400. The presence of a sulfate group on the catalyst was the most important factor in determining the catalytic performance of sorbitol dehydration to isosorbide. This work suggests that CeSO-400 catalysts may play an important role in reducing reaction conditions.

KEYWORDS

Cerium (IV) sulfate; isosorbide; sorbitol; dehydration

1 Introduction

Isosorbide is a chemical compound produced from renewable resources including rice, cassava, cane, and corn. Presently, isosorbide is used to replace bisphenol-A (BPA) in the synthesis of plastics, epoxy resins, and other chemicals [1–5], as the use of BPA may cause harm to humans, particularly infants [6]. In medical applications, isosorbide is used as a precursor in isosorbide dinitrate medicine. For these reasons, many countries are interested in isosorbide production. In 2012, the global production capacity of isosorbide was approximately 9,750 tons a year, mainly in Asia (42%), Europe (32%), the Americas

(21%), and others (5%). The economic contribution of isosorbide to the world economy grew from 73.8 million USD in 2014 to 324.6 million in 2020, i.e., 78% [7], and it has been predicted that it will grow to 703.1 million USD by 2027 [8]. A major isosorbide producer is Roquette from France with a production capacity of 20,000 tons/year using corn, wheat, and cassava as raw materials [9]. This producer uses a process carried out under a vacuum pressure of approximately 0.01 bar, using sulfuric acid [10]. This process produces an isosorbide yield of 77% of the raw material at 130°C. It is known that isosorbide can be synthesized from biomass through a three-step process, namely, 1) enzymatic depolymerization of starch to glucose, 2) hydrogenation of glucose to sorbitol, and 3) dehydration of sorbitol to isosorbide (Scheme 1) [11]. The conversion of starch to sorbitol (by Steps 1 and 2) is well-known and recognized as an economical process. However, the double dehydration of sorbitol into isosorbide has a high production cost due to the high energy consumption of generating and maintaining the vacuum environment. The production of isosorbide in vacuum conditions requires a large amount of energy both to continuously maintain a high vacuum level and to evaporate water obtained by the hydrogenation of glucose from the sorbitol solution [12]. Aricò et al. [13] reported the synthesis of isosorbide using a homogeneous catalyst in a reflux system at 90°C, with an isosorbide yield of 98%. Dimethyl carbonate was used as a solvent and a reagent, which was activated by 1,5-diazabicyclo (5.4.0) undec-5-ene (DBU). However, dimethyl carbonate is flammable. This study proposes a method of carrying out the reactions under high pressure to replace the vacuum and reflux techniques described above. However, this high-pressure reaction takes place under more severe conditions than the vacuum reaction, and the selection of an appropriate catalyst is very important when operating in a high-pressure reaction.

The heterogeneous catalysts used in sorbitol dehydration can be divided into three groups: ion exchange resins, zeolite, and metal compounds. An ion-exchange resin catalyst was investigated by Yamaguchi et al. [14]. They found that the resin catalyst denoted as Amberlyst-70 at the ratio of 1 g per 40 g sorbitol solution gave an isosorbide yield of 60.2% at 190°C and 16 h reaction time under H_2 gas at 50 bar. Using resin catalysts has a disadvantage in that the catalysts themselves have low thermal stability. Sulfonate groups can be broken in the temperature range of just 110°C–140°C [15]. As a result, the catalyst cannot be reused. Otomo et al. [16] studied the dehydration of aqueous sorbitol solution using a zeolite catalyst and found that H-beta (75) showed high performance, promoting a 76% isosorbide yield at 200°C after 18 h. However, the zeolite catalyst also has a drawback as it has a hydrophilic surface, thus creating competition between water and sorbitol for the active sites on the catalyst surface. The last group of catalysts is the metal compounds. He et al. [17] obtained isosorbide from cellulose with 47% yield using a nickel-niobium phosphate catalyst at 200°C for 24 h under H_2 gas at 30 bar. They found that the acidity of both Lewis and Brønsted acid sites plays a critical role in the catalytic performance of dehydration reactions. P-OH or Nb-OH groups represent Brønsted acid sites, and Nb species represent Lewis sites. In addition, Guo et al. [18] suggested that Lewis acid sites can convert the O-H bond of water formed during the reaction into Brønsted acid sites (H^+) to promote dehydration. Thus, the previously discussed work indicates that the use of metal compounds as catalysts leads to high catalytic activities. Recently, cerium has attracted much attention due to its remarkable advantages, such as, stability, availability, and inexpensiveness. Moreover, it has been reported that cerium can be extracted from waste [19–21]. The hydrophobicity of cerium is also beneficial in the protection of water during a reaction [22]. The use of metal sulfates in sorbitol dehydration has been documented by some researchers. For example, nickel sulfate, copper sulfate, and aluminum sulfate were used by Xia et al. [23], and Tin (II) sulfate by Dabbawala et al. [24]. They found that the acidity of the metal sulfate catalysts could be improved by calcination at 300°C–700°C.

To our knowledge, the use of cerium sulfate for sorbitol dehydration to obtain isosorbide has not been investigated. It is interesting to improve the acidity of cerium sulfate by calcination. In this study, cerium (IV) sulfate was calcined at different temperatures and used as a catalyst in sorbitol dehydration in a high-pressure

reaction to produce isosorbide. The influence of calcination temperature, reaction time, and catalyst amount on sorbitol conversion and isosorbide yield was investigated.

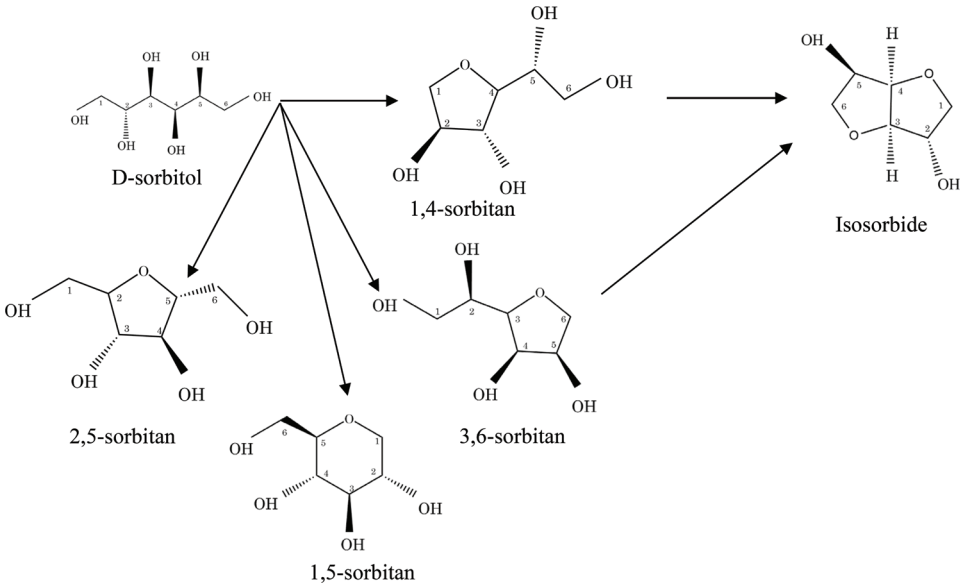

Scheme 1: Reaction pathways for the sorbitol dehydration reaction.

2 Experimental

2.1 Materials

Cerium (IV) sulfate tetrahydrate ($Ce(SO_4)_2{\cdot}4H_2O$) and cerium oxide (CeO_2) were purchased from Panreac and Soekawa chemicals, respectively. Aqueous D-Sorbitol solution containing 70 wt% sorbitol was purchased from Lab valley limited partnership (Thailand). The high-performance liquid chromatography (HPLC) standard solutions of 1,5-sorbitan, Isosorbide (98%), and D-Sorbitol (99%) were purchased from Sigma-Aldrich. In addition, 1,4-sorbitan was purchased from Sigma.

2.2 Catalyst Preparation

Cerium (IV) sulfate was prepared by calcining for 4 h in a furnace at a calcination temperature of 300°C, 400°C, 450°C, 500°C, or 650°C. The calcined catalysts are denoted as CeSO-T (where T is calcination temperature).

2.3 Catalyst Characterization

The crystalline phases of the catalysts were analyzed by X-ray diffractometry (XRD; Model D8 Advance, Bruker BioSpin AG, Germany) over a 2θ range of 5°–90° with a scan rate of 0.02°/s. Fourier transform infrared spectroscopy (FT-IR; Model Alpha II, Bruker, USA) was used for the identification of the functional groups of the catalyst over a range of 4000–550 cm^{-1}. The sulfur content was analyzed using an S elemental analyzer (LECO; LECO 628 series) on the Vario EL CUBE instrument and calculated by the difference in mass. Thermogravimetric analysis (TGA) was performed using a Shimadzu, TGA 50. It was measured from 30°C to 1000°C with a constant heating rate of 10°C/min under 40 mL/min airflow. Field-Emission Scanning Electron Microscopy (FE-SEM; 15 kV; Model: MIRA, TESCAN) was performed at a resolution of 50 μm. The oxidation state of the catalyst was measured using X-ray photoelectron spectroscopy (XPS; ULVAC-PHI, PHI 500 VersaProbe II)

equipped with Al Kα radiation as the excitation source. The binding energy shifts of the XPS were calibrated using the C 1s peak at 284.8 eV. The catalyst acidity was determined using ammonia temperature-programmed desorption (NH_3-TPD). First, the prepared catalyst was pretreated at 400°C for 2 h using helium at a constant flow rate of 50 mL/min and then cooled to 50°C. After pretreatment, 5 vol% of ammonia in helium at a constant flow of 50 mL/min flowed through the sample for ammonia adsorption for 1 h. Next, the ammonia desorption was performed under a helium flow rate of 50 mL/min from 50°C to 1000°C at a heating rate of 10°C/min. Finally, a thermal conductivity detector (TCD) was used to detect the amount of desorbed ammonia.

2.4 Catalytic Reaction

The sorbitol dehydration was performed in a high-pressure reaction (100 mL Teflon autoclave). The calcined catalyst and 50 mL of 70 wt% sorbitol were loaded into the reactor. After purging and pressuring to an initial pressure of 20 bar with nitrogen, the reactor was heated to the evaluated temperature and stirred at a constant speed of 550 rpm for an evaluated time. After the reaction, the reactor was cooled until the pressure reached 20 bar. The reactant and product concentrations were analyzed by HPLC (Shimadzu, LC-20AD, RI (RID-20 A) detector) with a Phenomenex Rezex RCM-monosaccharide column (8%; Ca^{2+}, 300 mm × 7.80 mm, mobile phase: water at 0.6 mL/min, 85°C). The following equations were used to calculate the sorbitol conversion (1) and product yield (2) based on the carbon mole balance.

$$\text{Sorbitol conversion } (\%) = \frac{\text{moles of reacted sorbitol}}{\text{moles of initial sorbitol}} * 100 \quad (1)$$

$$\text{Product yield } (\%) = \frac{\text{moles of product}}{\text{moles of initial sorbitol}} * 100 \quad (2)$$

The reusability of the catalysts was also investigated. The recovered catalyst was washed with DI water and then soaked in ethanol for 4 h at 30°C. After a specified time, the solid catalyst was separated by a centrifuge. Finally, the catalyst was dried at room temperature overnight.

3 Results and Discussion

3.1 Catalyst Characterization

The cerium (IV) sulfate tetrahydrate ($Ce(SO_4)_2{\cdot}4H_2O$) was analyzed for thermal decomposition by TGA. The analysis temperature was in the range of 30°C–1000°C as shown in Fig. 1. It should be noted that four stages of weight loss are observed at 80°C–140°C, 140°C–300°C, 400°C–600°C, and 700°C–920°C. The weight losses for the first two stages are 8% and 10.5%, respectively, arising from the loss of the four water molecules, similar to the decomposition of α-$Ce(SO_4)_2{\cdot}4H_2O$ reported by Casari et al. [25]. It is worth noting that it can be shown that the weight loss would be 17.81% if the four water molecules were removed from $Ce(SO_4)_2{\cdot}4H_2O$. By 400°C, the calcined catalyst, $Ce(SO_4)_2{\cdot}4H_2O$, was completely dehydrated to $Ce(SO_4)_2$ (anhydrous cerium (IV) sulfate or ceric sulfate), as reported in other studies [26,27]. In the third stage, a weight loss of approximately 12% is obtained due to the decomposition of the anhydrous cerium sulfate [28]. In the last stage, at temperatures of 700°C–920°C, the decomposition of the sulfate group, resulting in the formation of CeO_2, was considered to take place [29]. A calcination temperature of more than 700°C led to sulfate decomposition, decreasing the total acid sites as well as the catalyst acidity. Taking this into account, it was decided to calcine the $Ce(SO_4)_2{\cdot}4H_2O$ catalyst at 300°C, 400°C, 450°C, 500°C, and 650°C in this study.

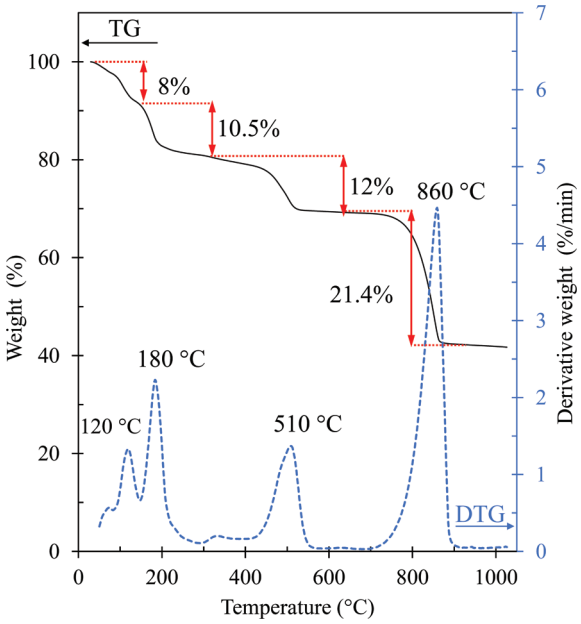

Figure 1: TG-DTG curves of $Ce(SO_4)_2{\cdot}4H_2O$

The XRD patterns of CeO_2 and the catalyst calcined at different temperatures are shown in Fig. 2. From the figure, it is evident that the presence of a pure CeO_2 peak is not observed in the calcined catalysts represented by curves (c)–(g). The data indicates that catalyst calcination at the selected temperatures has not changed them to a cerium oxide form. A comparison of the change in the catalyst before (b) and after (c–g) calcination was made. It was found that the crystallinity of $Ce(SO_4)_2{\cdot}4H_2O$ was changed after calcination, and that increasing the calcination temperature further changed the crystalline phase. As observed in the XRD patterns, the calcined catalysts can be divided into two groups: those calcined at 300°C–400°C (CeSO-300 and CeSO-400) and those at 450°C–650°C (CeSO-450, CeSO-500, and CeSO-650). In addition, grouping by crystallinity in this way also corresponds to the colors of the catalysts which were yellow for 300°C–400°C, and white for 450°C–650°C. As indicated in the figure, the CeSO-300 and CeSO-400 catalysts show diffraction peaks corresponding to $Ce(SO_4)_2$ [26], whereas the CeSO-450, CeSO-500, and CeSO-650 catalysts show peaks corresponding to $Ce_2(SO_4)_3$ (JCPDS 01-0208) and $CeOSO_4$ (JCPDS 39-0515) [30]. Moreover, calcination at 650°C also shows the phase of $CeOSO_4$ more clearly, which indicates that the structure of $Ce_2(SO_4)_3$ decomposes to $CeOSO_4$. This result should be compared with the work of Poston et al. [29], who reported that $Ce(SO_4)_2$ decomposes into two phases, $Ce_2(SO_4)_3$ and $CeOSO_4$, when the calcination temperature reaches 550°C, with only the $CeOSO_4$ phase being obtained at 600°C. In this study, the combined phase of the two compounds exists until the calcination temperature reaches 650°C. The XRD patterns thus indicate that the calcination temperature affects the crystalline phase changes of the catalyst.

The functional groups on the surface of cerium sulfate after calcination were identified using FT-IR spectra. Fig. 3 shows the FT-IR spectra of all the samples, which exhibit peaks at 3175, 1623, 1100, 981, and 593 cm^{-1}. These results are similar to those of Sahoo et al. [31]. The broad peaks at 3175 and 1623 cm^{-1} are assigned to the OH-groups stretching and bending vibrations, respectively (H_2O-bending). The broad peaks at 1100 and 981 cm^{-1} are attributed to the undistorted SO_4^{2-} tetrahedron. The absorption band at 593 cm^{-1} is assigned to S–O or S=O stretching in SO_4^{2-} [32]. After calcination, the bands originating from water and hydroxyl groups decrease, disappearing at 450°C, which is consistent with the results of the thermal analysis studies. The two absorption bands at 1100 and 981 cm^{-1} gradually merge into a single peak at 981 cm^{-1} by 500°C.

These results indicate that the S ions interact with the Ce ions and OH-groups on the catalyst surface. The sulfate group might be bonded to either one or two metals on the catalyst surface via oxygen atoms.

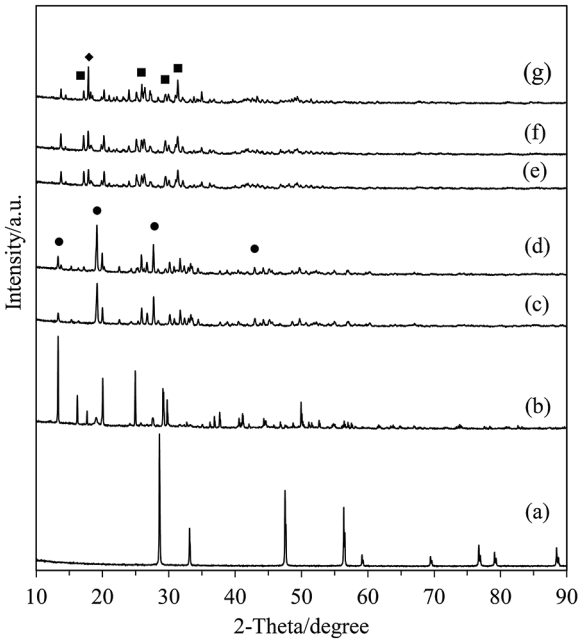

Figure 2: XRD patterns of the catalysts; (a) CeO_2, (b) $Ce(SO_4)_2$•$4H_2O$, (c) CeSO-300, (d) CeSO-400, (e) CeSO-450, (f) CeSO-500, (g) CeSO-650. ●: $Ce(SO_4)_2$, ▪: $Ce_2(SO_4)_3$, ♦: $CeOSO_4$

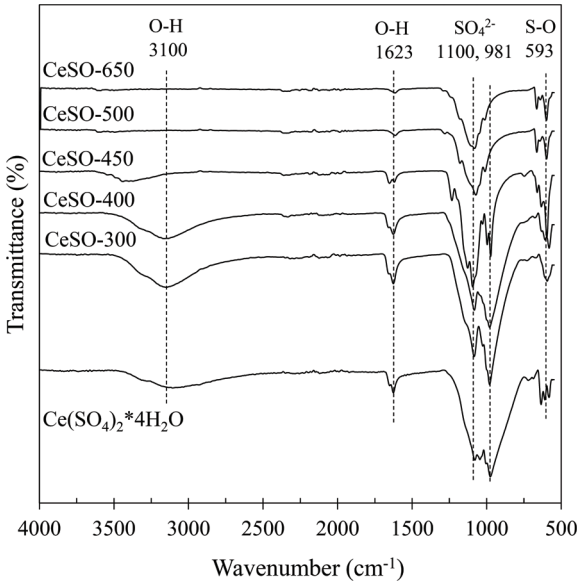

Figure 3: FTIR spectra of cerium (IV) sulfate calcined at different temperatures

FE-SEM images of the catalysts before and after calcination are presented in Fig. 4. $Ce(SO_4)_2$·$4H_2O$ (Fig. 4a) and CeSO-300 (Fig. 4b) have similar lump shapes. The lump shape changes to a somewhat

rod-like shape at increased calcination temperatures. As the calcination temperature increases, agglomeration of water on the surface decreases [24], causing the lump shape to change to a rod-like one. This is in agreement with the result of the TGA at 400°C, which shows that the catalyst is completely anhydrous, however, the FTIR spectra still showed an -OH group signal. At 650°C, the numerous rod-like shapes are observed to fracture into smaller pieces of various shapes. Evidently, the calcination temperature affects the morphology of the catalyst. The changes in shape and surface morphology of the catalysts at higher temperatures are evident of the phase conversion from Ce(IV) sulfate to Ce(IV) oxide.

The sulfur content of the calcined catalysts was measured by two different methods, namely sulfur elemental analysis and FE-SEM with Energy Dispersive X-Ray Spectroscopy (FE-SEM/EDX), with the data presented in Table 1. Both methods yield similar data and reveal that the amount of sulfur does not significantly change with the calcination temperature. It should be noted here that other studies reported that the sulfate disappeared at a temperature greater than 800°C [33]. In the previously discussed XRD results, a crystalline structure change of the catalyst was observed, suggesting some loss of sulfur from the catalyst. However, Table 1 reveals an almost constant amount of sulfur on the surface. Taking these results into consideration, it was thought that the sulfate might decompose to other forms on the surface of the catalyst. The NH_3-TPD analysis was used to determine the acid amount and acid strength distribution of the catalysts. The NH_3-TPD spectra of the catalysts are shown in Fig. 5. The NH_3-TPD spectra show a single peak in the temperature range of 750°C–850°C, which can be attributed to the presence of strong acid sites, which Dussenne et al. [34] confirmed are beneficial for protonating the hydroxyl groups of sorbitol. The number of acidic sites of CeSO-400, CeSO-450, CeSO-500, and CeSO-650 was 616.0, 764.2, 765.3, and 793.8 mmol g^{-1}, respectively. These results show that increasing calcination temperatures only slightly increase the acidity of the catalyst. The NH_3-TPD test reveals a fairly constant quantity of sulfur, in agreement with Table 1 and the XRD patterns.

It is known that acidity is an important parameter for dehydration reactions. In this study, the acidic properties (strength and amount) of the catalyst did not significantly change with the calcination temperature. The changes in the oxidation states of Ce, S, and O for the catalysts were determined by XPS, with the results presented in Fig. 6. The Ce 3d binding energy of the CeSO-400–650 catalysts are presented in Fig. 6a, where 887.2–886.2 and 905–903 eV represent $3d_{5/2}$ and $3d_{3/2}$, respectively [29]. These results indicate multiple oxidation states, with Ce potentially being +3 or +4. The analysis of Ce 3d of the catalysts revealed no significant change within the calcination temperature range of 400°C–650°C. This seems to indicate that cerium valency does not depend on calcination. The S 2p results of CeSO-400, CeSO-450, and CeSO-650 are displayed in Fig. 6b. The XPS spectra of S 2p can be deconvoluted by the magic plot program into three peaks. The two peaks at 168.5 and 169.9 eV, which are the S $2p_{3/2}$ and S $2p_{1/2}$ orbital peaks, represent sulfur in SO_4^{2-}, in which the sulfur oxidation is S^{6+} [35]. In addition, the low-intensity peak at 167 eV, which disappears at 450°C, is attributed to S^{4+} of SO_3^{2-} [36,37]. The peak observed at 170.7 eV is associated with an oxidized form of sulfur [29]. It should be noted that the crystalline structural change of the catalyst at 450°C correlates with the TGA and XRD data. The peak of SO_4^{2-} significantly decreases in intensity and shifts to lower binding energy, indicating that the polar reaction between S-O decreases when calcinated at 450°C. This shows that the sulfate species might be another form, existing as chelating bridged bidentate SO_4^{2-} ions, bidentate SO_4^{2-} ions, or interstitial SO_4^{2-} ions. The O 1s spectra are presented in Fig. 6c, clearly exhibiting three different oxygen species at the binding energies of 531.9, 532.9, and 534.9 eV. These peaks were ascribed to metal-oxygen bonds, sulfur–oxygen bonds and bridged oxygens of the surface hydroxyl groups, respectively [38]. Based on these data, it was concluded that the ligand SO_4^{2-} surrounding the metal ion changed after calcination.

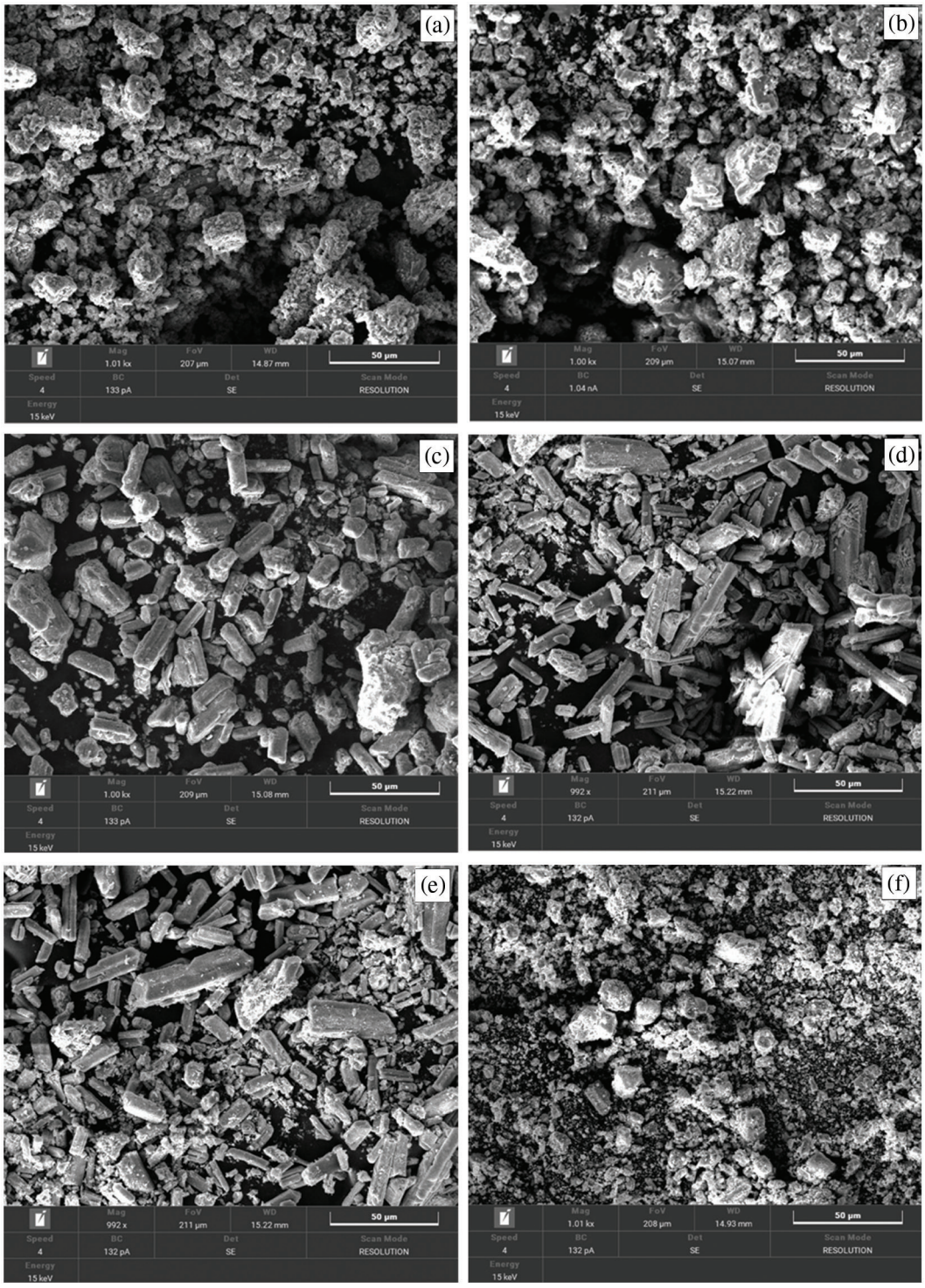

Figure 4: SEM images of (a) $Ce(SO_4)_2 \cdot 4H_2O$, (b) CeSO-300, (c) CeSO-400, (d) CeSO-450, (e) CeSO-500, and (f) CeSO-650

Table 1: Sulfur content of cerium (IV) sulfate calcined at different temperatures

Catalyst	S content (%)	
	S elemental analysis	FE-SEM/EDX
$Ce(SO_4)_2 \cdot 4H_2O$	16.8	16.8
CeSO-300	16.2	16.6
CeSO-400	16.9	16.6
CeSO-450	16.5	15.5
CeSO-500	16.9	16.3
CeSO-650	16.7	16.1

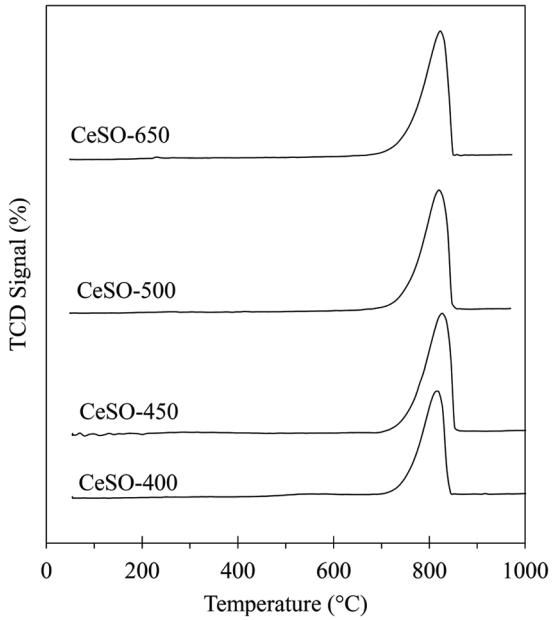

Figure 5: NH_3-TPD profiles of the cerium (IV) sulfate calcined at different temperatures

3.2 Catalytic Sorbitol Dehydration

The efficiency of the sorbitol dehydration under high-pressure reaction conditions using the cerium sulfate catalysts calcined at different temperatures was evaluated. HPLC was used to identify the products of sorbitol dehydration. Three distinct peaks were identified: sorbitol, isosorbide, and 1,4-sorbitan, but 1,5-sorbitan was not found. Therefore, the peaks that could not be identified were treated as unknowns. Sorbitol dehydration was carried out under the following conditions: 180°C for 6 h, 2 g of catalyst in 50 mL of 70 wt% sorbitol. As shown in Table 2, the catalytic performance can be divided into 2 groups according to the characteristics previously classified and discussed. The first group comprises CeSO-300 and CeSO-400, which yielded similar results. They achieve the full conversion of sorbitol with an isosorbide yield of 57.7%. The second group comprises CeSO-450, CeSO-500, and CeSO-650. The catalysts in this group are the most active in converting sorbitol to 1,4-sorbitan in the first-step dehydration. In the second-step dehydration, however, they only produce ~2% isosorbide. It is thus shown that the cerium (IV) sulphate calcined at 300°C and 400°C gives higher yields than that calcined at 450°C, 500°C, and 600°C. From these experimental results, it is found that the crystalline structure and

sulfate species of the catalyst might account for the different catalytic activities. Based on these observations, the crystalline structure changes in the XRD and XPS indicate a change in the interactions between the metal and sulfate bonds. These results correspond to the work of Takeshita et al. [39] who found that the calcination temperature has a large effect of the ions surrounding the metal. Comparing CeSO-300 and CeSO-400, the CeSO-400 catalyst provides the best isosorbide synthesis efficiency. This is due to the fact that fewer undesired by-products are formed, thus providing a higher yield of 1,4-sorbitan which can be changed to isosorbide in the second dehydration.

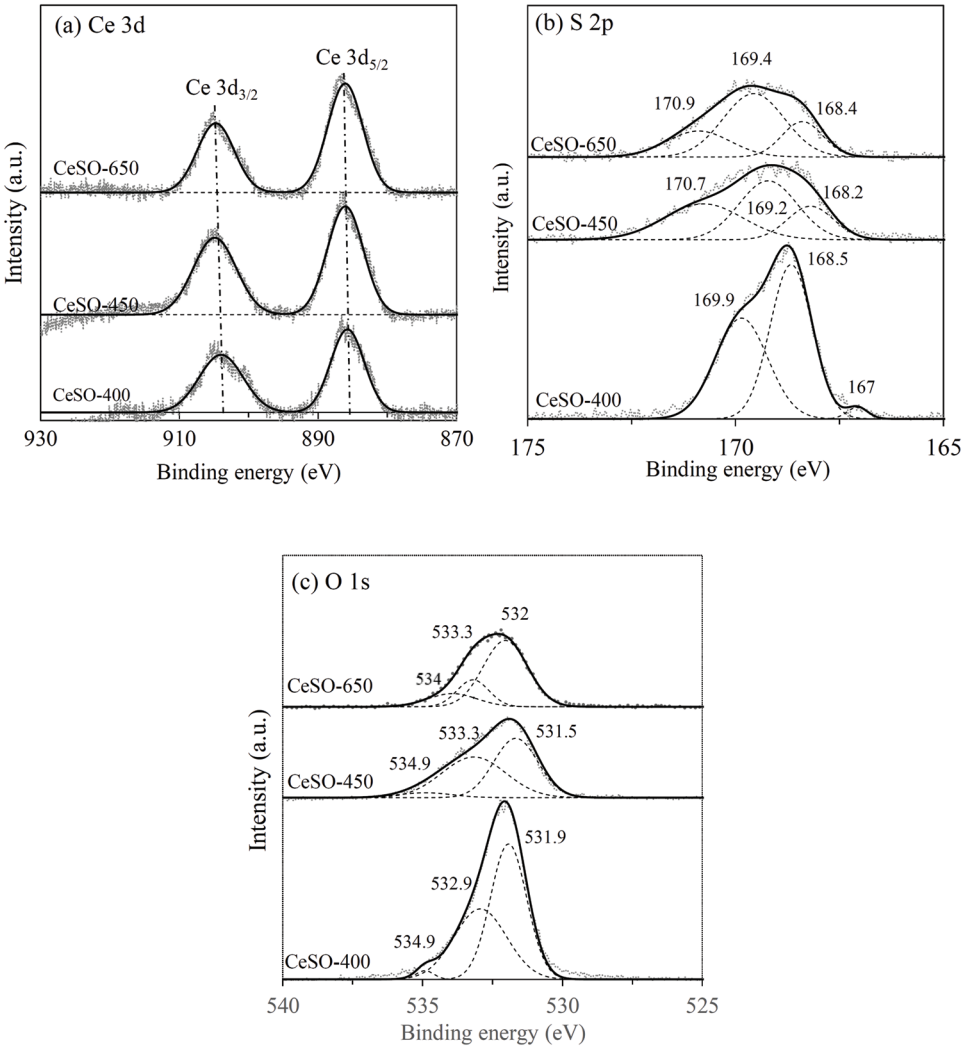

Figure 6: XPS spectra of the catalysts; (a) S 2p, (b) Ce 3d and (c) O 1s

After identifying the best calcination conditions for the catalyst, the CeSO-400 catalyst was analyzed to determine optimal reaction time and catalyst loading conditions, as shown in Fig. 7. The optimal reaction temperature was selected to be 180°C from a previous study [40]. Fig. 7a shows the complete conversion of sorbitol at all times. However, the reaction still needed residence time to convert 1,4-sorbitan to isosorbide. It can be seen that the 1,4-sorbitan yield decreases when the reaction time increases, whereas the isosorbide yield increases with the reaction time, reaching 57.7% after 6 h and remaining stable until 8 h. This evidently shows that 1,4-sorbitan is an intermediate of the reaction. At 8 h, The 1,4-sorbitan

yield was somewhat stable, showing that 1,4-sorbitan does not further convert to isosorbide at a long reaction time [41]. Thus, the optimal reaction time was selected to be 6 h. The effect of catalyst loading was studied in the range of 0.5–2.5 g with a reaction time of 6 h. Fig. 7b shows that increasing the amount of loaded catalyst increases the isosorbide yield, reaching a maximum at 2.5 g of CeSO-400. However, the increase in catalyst loading from 2 to 2.5 g only increases the yield by 5%. Thus, a dosage of 2 g was deemed the most suitable, with an acceptable yield. Thus, the optimal conditions for sorbitol dehydration to isosorbide in a high-pressure reaction in this study are a reaction temperature of 180°C for 6 h, using 2 g of CeSO-400. At these conditions, the sorbitol conversion and isosorbide yield are 100% and 57.7%, respectively.

Table 2: Performance of calcined catalysts for sorbitol dehydration[a]

Run order	Catalyst	Conversion (%)	Product yield (%)		
			1,4-sorbitan	Isosorbide	Unknown
1	CeSO-300	100	10.2	57.7	32.1
2	CeSO-400	100	14.3	57.7	28.0
3	CeSO-450	62.0	28.7	2.1	9.4
4	CeSO-500	63.8	27.8	2.4	10.5
5	CeSO-650	66.0	27.4	2.2	13.9

Note: [a] Reaction conditions: 70 wt% sorbitol 50 mL, catalyst 2 g, 180°C, 20 bar, 6 h.

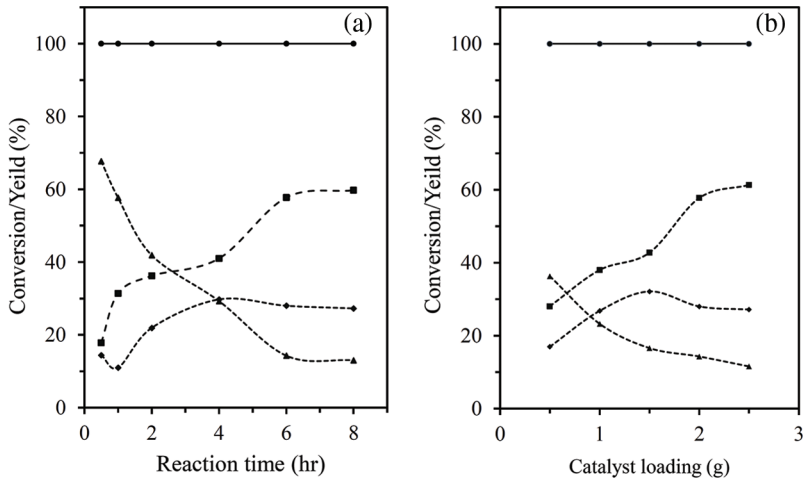

Figure 7: Catalytic sorbitol dehydration over CeSO-400 with a) different reaction times (180°C, 2 g) b) different catalyst loading (180°C, 6 h); (●) sorbitol conversion, (▲) 1,4-sorbitan yield, (▪) isosorbide yield, (♦) unknown yield

To further evaluate this method, we compared our results with those of other methods used for the synthesis of isosorbide in high-pressure reactions, as shown in Table 3. From the table, it can be seen that the CeSO-400 catalyst has lower catalytic efficiency for producing isosorbide than three catalysts, namely $ZnCl_2$, boron phosphate, and H-beta (75). To reiterate, the CeSO-400 catalyst obtained 100% sorbitol conversion and a 57.7% isosorbide yield after 6 h at 180°C. In comparison, the $ZnCl_2$ catalyst achieved a 27.3% higher isosorbide yield but the cost of the catalyst was more than 86% greater. The boron phosphate catalyst used more severe conditions, with similar conditions to those in this study (180°C, 8 h)

only resulting in 77.9% sorbitol conversion and 11.7% isosorbide yield. The last H-Beta (75) catalyst was also used under more severe conditions and required more expensive materials. Based on our literature search, it seems that our method offers the best performance (high yields, low temperature, short reaction time, and lower cost) in the conversion of sorbitol to isosorbide. It would be of interest to study the purification of the synthesized product in future work to obtain high purity isosorbide.

Table 3: Comparison of CeSO-400 with other catalysts used for sorbitol dehydration

Catalyst	Temp. (°C)	Time (h)	%wt g catalyst/g sorbitol	Sorbitol conv. (%mol)	Isosorbide yield (%mol)	Ref.
$ZnCl_2$	200	4.5	1200	n.r.	85	[42]
Boron phosphate	250	8	1	99.5	79.9	[43]
Boron phosphate	180	8	1	77.9	11.7	[43]
Cerium phosphate	200	2	1	57.3	7.9	[43]
Activated carbon-supported nickel oxide (Ni/AC-II-B)	250	6	0.26	91.32	28.87	[44]
H-beta (75)	200	12	n.r.	>99	77	[16]
CeSO-400	180	6	5	100	57.7	This work

The reusability of the CeSO-400 catalyst was also of interest and investigated for sorbitol dehydration under high pressure at 180°C for 6 h. After the spent catalyst was separated by centrifugation and dried at 100°C, it was reused in the dehydration process. In other experiments, the catalyst was reclaimed and renewed by soaking in ethanol for 4 h, filtered and dried at room temperature, and then reused in the process. In other words, the reclaimed catalyst was reused in both washed and unwashed forms. The results of these experiments are presented in Table 4, which shows that sorbitol conversion decreases from 100% to 36% after the first run with a fresh catalyst. The process yielded 21% 1,4-sorbitan and no isosorbide. For this reason, the catalyst was washed with ethanol because it was thought that the surface of the spent catalyst could have deposited coke covering the active sites. The presence of coke was confirmed by TGA analysis, as shown Fig. 8. However, the washed catalyst yielded only slightly different sorbitol conversion (39% as compared with 36%), and no isosorbide similar to the unwashed catalyst. Therefore, coke covering the active sites was not necessarily the main reason for the zero isosorbide yield. It was then thought that the loss of active sites as a result of the loss of sulfate could be the main cause for the zero isosorbide yield. To verify this, this loss of active sites was investigated by FT-IR, with the spectra shown in Fig. 9. The spectra of the spent catalyst washed with ethanol show a low intensity of the broad peaks at 1100 and 981 cm^{-1}, attributed to SO_4^{2-}. This data indicates that the cause of the deactivation of the CeSO-400 catalyst might be the loss of sulfate. Based on these results, it can be seen that the presence of the sulfate group on the catalyst is the most important factor in determining the catalytic performance for the dehydration of sorbitol to isosorbide under high pressure.

Table 4: Reusability of CeSO-400 for sorbitol dehydration

Entry	Catalyst	Conversion (%)	Yield of product (%)		
			1,4-sorbitan	isosorbide	unknown
1	Fresh CeSO-400	100	14.3	57.7	28.0
2	Unwashed CeSO-400 spent 1	36	21	0	15
3	Washed CeSO-400 spent 1 (EtOH)	39	21	0	18

Note: Reaction conditions: catalyst 2 g, 20 bar, 180°C, 6 h.

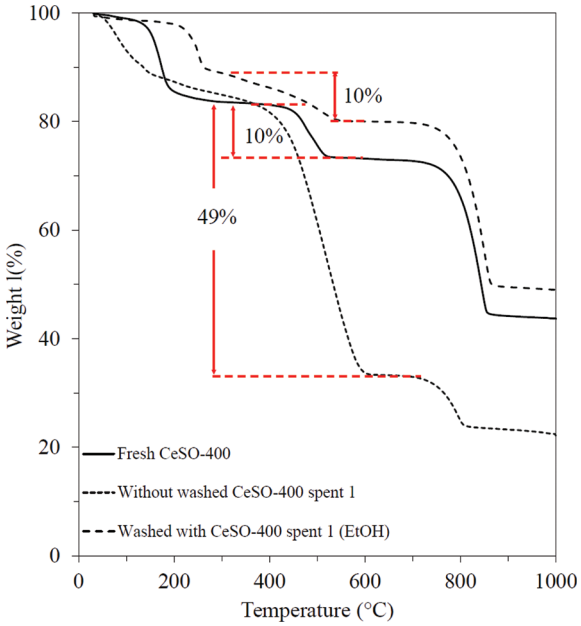

Figure 8: TG curves of fresh CeSO-400 catalyst and spent catalysts (washed and unwashed)

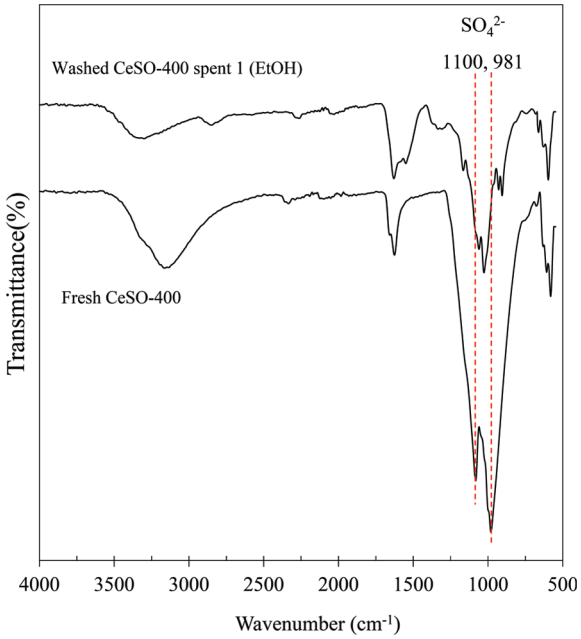

Figure 9: FT-IR spectra of fresh CeSO-400 catalyst and washed CeSO-400 spent 1 (EtOH) catalyst

4 Conclusion

The presented method, using a cerium-based catalyst derived from cerium (IV) sulfate, was more energy-efficient than other catalysts due to milder reaction conditions. The catalysts calcined at different temperatures exhibited different crystalline structures and sulfate species, yielding different efficiencies for converting sorbitol to isosorbide. The CeSO-400 catalyst resulted in the complete conversion of sorbitol with an isosorbide yield of 57.7% after 6 h at 180°C. The presence of a sulfate group on the

catalyst was the most important factor in determining the catalytic performance of sorbitol dehydration to isosorbide. In addition, the stability of CeSO-400 was investigated, and it was discovered that the spent catalyst could not be reused due to the loss of sulfate.

Funding Statement: The authors appreciative and acknowledge the Faculty of Engineering, Khon Kaen University, Thailand, and the Graduate School, Khon Kaen University, Thailand, for supporting the Lecturer in Admitting High Potential Students to Study and Research in His Expert Program Year 2018 (Grant No. 611JT212) for financial support. The authors also thank the Synchrotron Light Research Institute (Public Organization), Thailand, for technical support on the XPS measurements. In addition, the authors would like to thank the CAT-REAC Industrial Project at Chulalongkorn University, Pathumwan, Bangkok, for their facilities and financial support.

Conflicts of Interest: The authors declare that they have no conflicts of interest to report regarding the present study

References

1. Guo, W., Cai, W., Wang, D., Wang, J., Zhu, X. et al. (2022). Halogen-free flame retarded poly(Lactic acid) with an isosorbide-derived polyphosphonate. *Journal of Renewable Materials, 10(7),* 1875–1888. https://doi.org/10.32604/jrm.2022.018823
2. Aricò, F. (2020). Isosorbide as biobased platform chemical: Recent advances. *Current Opinion in Green and Sustainable Chemistry, 21,* 82–88. https://doi.org/10.1016/j.cogsc.2020.02.002
3. Gómez-de-Miranda-Jiménez-de-Aberasturi, O., Centeno-Pedrazo, A., Fernández, S. P., Alonso, R. R., Medel, S. et al. (2021). The future of isosorbide as a fundamental constituent for polycarbonates and polyurethanes. *Green Chemistry Letters and Reviews, 14,* 533–543. https://doi.org/10.1080/17518253.2021.1965223
4. Russo, F., Galiano, F., Pedace, F., Aricò, F., Figoli, A. (2020). Dimethyl isosorbide as a green solvent for sustainable ultrafiltration and microfiltration membrane preparation. *ACS Sustainable Chemistry and Engineering, 8(1),* 659–668. https://doi.org/10.1021/acssuschemeng.9b06496
5. Qian, W., Tan, X., Su, Q., Cheng, W., Xu, F. et al. (2019). Transesterification of isosorbide with dimethyl carbonate catalyzed by task-specific ionic liquids. *ChemSusChem, 12(6),* 1169–1178. https://doi.org/10.1002/cssc.201802572
6. Mohapatra, P., Rajankar, P. (2019). Bottles can be toxic–Part II. https://www.toxicslink.org
7. Grand View Research (2020). Resource Circulation Equipment Market Size, Share & Trends Analysis Report by Application, by Region (North America, Europe, Asia Pacific, RoW), and Segment Forecasts, 2015–2020. http://www.grandviewresearch.com/industry-analysis/resource-circulation-equipment-market
8. Global Industry Analysts (2022). Global isosorbide industry. https://www.reportlinker.com/p05957183/Global-Isosorbide-Industry.html?utm_source
9. Stichnothe, H., JØrgensen, H., de Bari, I., Haveren, J. V. (2020). *Bio-based chemicals: A 2020 update*. Italy: EA Bioenergy.
10. Song, I. H., Kim, T. S., Son, S. R., Yim, Y. J., Hong, S. J. (2017). *Method of preparing anhydrosugar alcohol by two-step reaction*. Patent No: US 2017/0057974 A1.
11. Bonnin, I., Mereau, R., Tassaing, T., de Oliveira Vigier, K. (2020). One-pot synthesis of isosorbide from cellulose or lignocellulosic biomass: A challenge? *Beilstein Journal of Organic Chemistry, 16,* 1713–1721. https://doi.org/10.3762/bjoc.16.143
12. Choi, Y. B., Lee, S., Son, S. R., Song, I. H. (2019). *Method for producing anhydrosugar alcohol by high-pressure reaction*. Patent No: US 2019/0241581 A1.
13. Aricò, F., Tundo, P. (2016). Isosorbide and dimethyl carbonate: A green match. *Beilstein Journal of Organic Chemistry, 12,* 2256–2266. https://doi.org/10.3762/bjoc.12.218

14. Yamaguchi, A., Sato, O., Mimura, N., Shirai, M. (2015). One-pot conversion of cellulose to isosorbide using supported metal catalysts and ion-exchange resin. *Catalysis Communications, 67(2),* 59–63. https://doi.org/10.1016/j.catcom.2015.04.009
15. Chakrabarti, A., Sharma, M. M. (1993). Cationic ion exchange resins as catalyst. *Reactive Polymers, 20(1–2),* 1–45. https://doi.org/10.1016/0923-1137(93)90064-M
16. Otomo, R., Yokoi, T., Tatsumi, T. (2015). Synthesis of isosorbide from sorbitol in water over high-silica aluminosilicate zeolites. *Applied Catalysis A: General, 505,* 28–35. https://doi.org/10.1016/j.apcata.2015.07.034
17. He, M., Guo, J., Wang, X., Song, Y., Liu, S. et al. (2020). Direct conversion of cellulose into isosorbide over Ni doped $NbOPO_4$ catalysts in water. *New Journal of Chemistry, 44(25),* 10292–10299. https://doi.org/10.1039/D0NJ01403F
18. Guo, J., Song, Y., Liu, S., Huang, L., Wang, X. et al. (2021). Sequential dehydration of sorbitol to isosorbide over acidified niobium oxides. *Catalysis Science & Technology, 11(12),* 4226–4234. https://doi.org/10.1039/D1CY00326G
19. Ilyas, S., Kim, H., Srivastava, R. R. (2021). Cleaner production of rare earth elements from phosphorus-bearing sulfuric acid solution of vein deposit monazite. *Journal of Cleaner Production, 278,* 123435. https://doi.org/10.1016/j.jclepro.2020.123435
20. Ilyas, S., Kim, H., Srivastava, R. R. (2021). Hydrometallurgical recycling of rare earth metal–cerium from bio-processed residual waste of exhausted automobile catalysts. *The Journal of the Minerals, 73(1),* 19–26. https://doi.org/10.1007/s11837-020-04471-3
21. Ilyas, S., Kim, H., Srivastava, R. R. (2021). Extraction equilibria of cerium (IV) with cyanex 923 followed by precipitation kinetics of cerium (III) oxalate from sulfate solution. *Separation and Purification Technology, 254,* 117634. https://doi.org/10.1016/j.seppur.2020.117634
22. Azimi, G., Dhiman, R., Kwon, H. M., Paxson, A. T., Varanasi, K. K. (2013). Hydrophobicity of rare-earth oxide ceramics. *Nature Materials, 12,* 315–320. https://doi.org/10.1038/nmat3545
23. Jiaojiao Xia, H. H., Yu, D., Hu, Y., Zou, B., Sun, P. et al. (2011). Sulfated copper oxide: An efficient catalyst for dehydration of sorbitol to isosorbide. *Catalysis Communications Journal, 12,* 544–547. https://doi.org/10.1016/j.catcom.2010.12.002
24. Dabbawala, A. A., Mishra, D. K., Hwang, J. S. (2013). Sulfated tin oxide as an efficient solid acid catalyst for liquid phase selective dehydration of sorbitol to isosorbide. *Catalysis Communications, 42,* 1–5. https://doi.org/10.1016/j.catcom.2013.07.020
25. Casaria, B. M., Langer, V. (2007). Two $Ce(SO_4)_2$ * $4H_2O$ polymorphs crystal structure. *Journal of Solid State Chemistry, 180,* 1616–1622. https://doi.org/10.1016/j.jssc.2007.02.017
26. Yang, Y., Yang, R. D. (1992). Study on the thermal decomposition of tetrahydrated cerie sulphate. *Thermochimica Acta, 202,* 301–306. https://doi.org/10.1016/0040-6031(92)85174-T
27. Tagawa, H. (1984). Thermal decomposition temperatures of metal sulfates. *Thermochimica Acta, 80,* 23–33. https://doi.org/10.1016/0040-6031(84)87181-6
28. Udupa, M. R. (1982). Thermal decomposition of cerium (IV), cerium (III), chromium (III) and titanium (IV) sulphates. *Thermochimica Acta, 57,* 377–381. https://doi.org/10.1016/0040-6031(82)80048-8
29. Poston, J. A., Siriwardane, R. V., Fisher, E. P., Miltz, A. L. (2003). Thermal decomposition of the rare earth sulfates of cerium (III), cerium (IV), lanthanum (III) and samarium (III). *Applied Surface Science, 214(1–4),* 83–102. https://doi.org/10.1016/S0169-4332(03)00358-1
30. Shi, Y., Tan, S., Wang, X., Li, M., Li, S. et al. (2016). Regeneration of sulfur-poisoned CeO_2 catalyst for NH_3-SCR of NO_x. *Catalysis Communications, 86,* 67–71. https://doi.org/10.1016/j.catcom.2016.08.004
31. Sahoo, S. K., Mohapatra, M., Singh, A. K., Anand, S. (2010). Hydrothermal synthesis of single crystalline nano CeO_2 and its structural, optical, and electronic characterization. *Materials and Manufacturing Processes, 25(9),* 982–989. https://doi.org/10.1080/10426914.2010.480995
32. Ramaswamy, V., Vimalathithan, R. M., Ponnusamy, V. (2010). Synthesis and characterization of nano particles thesis. *Advances in Applied Science Research, 3,* 197–204.

33. Sergent, N., Lamonier, J. F., Aboukais, A. (2000). Electron paramagnetic resonance in combination with the thermal analysis, X-ray diffraction, and Raman spectroscopy to follow the structural properties of $Zr_xCe_{1-x}O_2$ solid systems and precursors. *Chemistry of Materials, 12,* 3830–3835. https://doi.org/10.1021/cm000315d
34. Dussenne, C., Wyart, H., Wiatz, V., Suisse, I., Sauthier, M. (2019). Catalytic dehydration of sorbitol to isosorbide in the presence of metal tosylate salts and metallized sulfonic resins. *Molecular Catalysi, 463,* 61–66. https://doi.org/10.1016/j.mcat.2018.11.004
35. Dabbawala, A. A., Alhassan, S. M., Mishra, D. K., Jegal, J., Hwang, J. S. (2018). Solvent free cyclodehydration of sorbitol to isosorbide over mesoporous sulfated titania with enhanced catalytic performance. *Molecular Catalysis, 454,* 77–86. https://doi.org/10.1016/j.mcat.2018.05.009
36. Ferrizz, R. M., Gorte, R. J., Vohs, J. M. (2002). TPD and XPS investigation of the interaction of SO_2 with model ceria catalysts. *Catalysis Letters, 82(1–2),* 123–129.
37. Joseph Antony, K., Viswanathan, B. (2009). Single-step synthesis and structural study of mesoporous sulfated titania nanopowder by a controlled hydrolysis process. *ACS Applied Materials & Interfaces, 1(11),* 2462–2469. https://doi.org/10.1021/am900437u
38. Lu, C., Mu, S., Du, J., Zhang, K., Guo, M. et al. (2020). Investigation on the composition and corrosion resistance of cerium-based conversion treatment by alkaline methods on aluminum alloy 6063. *RSC Advances, 10(60),* 36654–36666. https://doi.org/10.1039/D0RA07201J
39. Takeshita, T., Ohnishi, R., Tanabe, K. (1974). Recent survey of catalysis by solid metal sulfates. *Catalysis Reviews, 8(1),* 29–63. https://doi.org/10.1080/01614947408071856
40. Boupan, M., Wongpakham, P., Sabangban, O., Theerakulpisut, S., Neramittagapong, A. et al. (2021). Catalytic performance of acid catalysts for sorbitol dehydration to isosorbide. *Journal of the Japan Institute of Energy, 100,* 206–211. https://doi.org/10.3775/jie.100.206
41. Yuan, D., Zhao, N., Wang, Y., Xuan, K., Li, F. et al. (2019). Dehydration of sorbitol to isosorbide over hydrophobic polymer-based solid acid. *Applied Catalysis B: Environmental, 240,* 182–192. https://doi.org/10.1016/j.apcatb.2018.08.036
42. Li, J., Spina, A., Moulijn, J. A., Makkee, M. (2013). Sorbitol dehydration into isosorbide in a molten salt hydrate medium. *Catalysis Science & Technology, 3,* 1540–1546. https://doi.org/10.1039/c3cy20809e
43. Rusu, O. A., Hoelderich, W. F., Wyart, H., Ibert, M. (2015). Metal phosphate catalyzed dehydration of sorbitol under hydrothermal conditions. *Applied Catalysis B: Environmental, 176–177,* 139–149. https://doi.org/10.1016/j.apcatb.2015.03.033
44. Li, H., Yu, D., Hu, Y., Sun, P., Xia, J. et al. (2010). Effect of preparation method on the structure and catalytic property of activated carbon supported nickel oxide catalysts. *Carbon, 48(15),* 4547–4555. https://doi.org/10.1016/j.carbon.2010.08.038